

Experimental Study and Computer Simulation of Fracture Toughness of Ni Base Superalloy Using CT Specimen

Muhammad Hasibul Hasan, Chahat Soi, Azin Mirzajavadkhan, Saba Rafieian and Mirt Mehany



Received: 16 September 2018
Accepted: 07 November 2018
Published: 01 December 2018
Publisher: Deer Hill Publications
© 2018 The Author(s)
Creative Commons: CC BY 4.0

ABSTRACT

Due to superior mechanical and metallurgical performance, Nickel-base Alloys 617 and 276 have been considered as structural material for used in complex and stochastic applications. Surface irregularities such as cracks in the material may be vulnerable to the structural integrity of an engineering component. Void growth behaviour is however analysed using crystal plasticity theory in nickel-based super alloys. Elastic-plastic fracture mechanics base single compact tension specimen has been used to determine the J_{IC} value as a function of temperature of austenitic Alloy 617 and 276 for ductile crack growth behaviour. Crack formation is appropriately explained through crack nucleation based on the microstructural heterogeneity properties of the alloys. Alloy 617 showed a fair increased resistance to fracture as temperature increased from ambient to 500°C for duplicate testing, satisfying the EPFM criteria. Whereas the J_{IC} values of Alloy 276 increased gradually with temperature up to 300° C and due to enhanced plasticity in the vicinity of 400° C this alloy shows inconsistent value. Two-dimensional simulation of J-integral model of these nickel base super alloys at temperature range 100°C to 500° C has been proposed. Particular focus is given on the load line displacement where crack propagation occurs during the loading phase only. Path independency of J-integral has been clearly demonstrated for both the alloys up to 300° C employing finite element analysis meshing with 1922 quadrilateral 2D solid elements in ANSYS. Cracks are typically initiated in relation to the level of strain range. A higher strain range initiates cracks due to precipitate shearing, whereas a low strain range initiates cracks with oxidation reactions and carbide diffusion. The values of K_{IC} and crack tip opening displacement for these alloys have been calculated based on the experimental data. Moreover, fracture morphology in the loading and unloading sequences near the crack tip has been analysed by SEM.

Keywords: Fracture Mechanics, Fracture Toughness, Superalloy, Computer Simulation

1 INTRODUCTION

1.1 Background

Due to a disparity in supply and demand, energy price is on the rise. Moreover, excessive use of fossil fuels produces pollutants. For these reasons, researchers are searching for alternative energy sources. Renewable energy is a promising sector as it is clean, available and cheap. Wind is a major source of renewable energy. Wind turbines are used to convert wind energy to electrical power. Currently, worldwide 40,000 MW power is produced from wind energy and it is predicted that the growth rate will be 30% in the next decade [1]. Alloy 617 and 276 were found appropriate to be used as wind turbine blade material. These alloys are also suitable for heat exchanging applications, such as in Next Generation Nuclear Plants (NGNP) [2]. Therefore, metallurgical characterization of these materials is necessary. Mechanical properties of a structure can be modified in many ways, for example: through the application of annealing, giving Alloy 617 resistance to degradation after long-term exposure [3]. In this paper, the behavior of Alloys 617 and 276 in terms of the metallurgical and mechanical properties are characterized based on the fracture toughness, particularly for wind turbine blade applications along with other conventional polyester glass fiber materials.

M. H. Hasan ✉, C. Soi, A. Mirzajavadkhan, S. Rafieian and M. Mehany
Department of Mechanical and Industrial Engineering
Ryerson University
350 Victoria Street, Toronto, ON M5B 2K3
Canada
Email: hasibulhasan@ryerson.ca

Reference: Hasan, M. H., Soi, C., Mirzajavadkhan, A., Rafieian, S. and Mehany, M. (2018). Experimental Study and Computer Simulation of Fracture Toughness of Ni Base Super Alloys Using CT Specimen. *International Journal of Engineering Materials and Manufacture*, 3(4), 224-236.

1.2 Material Selection

To be operated in harsh environments such as desert areas where dust and sandstorms are more commonly to happen, turbine blade material should sustain with high impact forces and abrasion. Impact velocity is determined by wind flow velocity and the blade’s speed of revolution. Due to the maximization of rotational speed at the leading edges of an aerofoil, an elastomeric material should be applied to prevent erosion. However, it is necessary to replace the tape frequently as they fail to satisfactorily absorb the concussion energy of the particulate matter. Hence, blade materials should be chosen carefully to prevent damages. Polyester-glass fibre blade material is suitable for high impact erosion. However, nickel-based superalloy has the potential to be used as it has a high tensile strength as well as corrosion resistance properties.

In 1970, Ni-base Alloy 617 was developed to be used in aerospace engineering as an advanced sheet material. The significant properties of this alloy are high strength, oxidation resistance at high temperature (980°C) as well as high resistance to both creep deformation and ruptures at temperatures up to 850°C [4]. In addition, it has excellent metallurgical stability and low density, which provides a high strength-to-weight ratio. Due to its oxidation resistance characteristics, Alloy 617 along with Alloy 276 are used in the production process of Nitric Acid, heat treating baskets and reduction boats in molybdenum refinement as catalyst-grid support [5]. Some other high-temperature applications of Alloy 617 are inducting, combustion cans, transition liners in gas-turbines, thermal energy storage capsules, manufacturing of retort furnace and gas cooled reactors. NASA has been using this Alloy material for heat shielding in space transportation systems.

1.3 Scope

An examination on tensile deformation of Alloy 617 and 276 under extensive variety of temperatures beginning from ambient to 1000°C had been completed by numerous agents [6]. Surface irregularities impact the basic integrity of metallic components. Control variables of development rate of surface irregularities and voids comprise of stress triaxiality, the underlying void volume fraction, lode parameters, the crystallographic orientation, the initiated slip system and the level of elastic anisotropy [7]. Variable stacking conditions are forced on these segments in temperamental desert conditions and dust storms. Elastic-Plastic-Fracture- mechanics (EPFM) was applied to appraise crack durability (fracture toughness) of this alloy at various temperatures [8], which happen contingent upon microstructural heterogeneities and the effect on behaviour-elastic anisotropy, morphology and crystallography with the idea of the enforced loading [9]. Numerical analysis has been finished by business programming ANSYS utilizing Finite element technique, in which conduct of crack deformations are delineated based microscopic and macroscopic structures in impact temperature reliance of yield strength [10]. In an investigation, specimens were tried by scanning electron microscopy (SEM) to decide the morphology of deficiency.

2 EXPERIMENTATION

2.1 Test Material

Alloy 617 was custom-melted at the Huntington Alloys Corporation, West Virginia by vacuum-induction-melting (VIM). Rectangular and round bars were fabricated using forging and hot-rolling. After the hot-rolling operation, the thickness of rectangular bars was reduced by cold-rolling. However, residual stresses were developed from hot and cold rolling operations, which were relieved further by thermal treatment. This thermal treatment consisted of solution-annealing at 2150°F (1175°C) for variable time periods depending on the thickness of the processed bars. It produces large sized austenitic grains in alloys. After heat treatment by solution-annealing at 1163°C (2125°F), rapid cooling was done which provides a fully austenitic microstructure. Table 1 and 2 provides the chemical composition and room temperature tensile properties of the material, respectively.

Table 1: Chemical Composition of Alloy 617 (HV1160) and 276 (Z7437CG) (wt %)

Heat No.	C	Mn	Fe	S	Si	Cu	Cr	Ni	Al	Ti	Co	Mo
HV1160	0.06	0.121	0.002	0.009	0.004	0.001	22.10	54.80	0.87	0.29	12.17	9.52
Z7437CG	0.006	0.42	5.9	0.001	0.008	-	15.8	58.3	-	-	0.1	15.9

Table 2: Ambient-Temperature Tensile Properties

Heat No.	Yield strength MPa	Ultimate tensile strength, MPa	%El	%RA	Hardness (R _B)
HV 1160	371	855	78.35	61.98	86.8
Z7437CG	354	794	87	60	79

2.2 Test Specimens

Fracture toughness (J_{IC}) of the alloy was determined by a compact-tension (CT) specimen of 25.4 mm thickness with a straight through notch. In the machining process, the longitudinal rolling direction was normal to the crack plane. Figure 1. describes the configuration and pictorial view of the test specimen.

2.3 Test Procedure

Test specimens and experimental setup were done as per the procedure prescribed by the ASTM Designation E 313-1989 [12]. Initially, test specimens were designed to evaluate the plane strain fracture toughness [11] based on the linear-elastic fracture- mechanics (LEFM) concept for Alloy 617 [12]. to comply with the LEFM criteria significantly thicker 20" compact tension (CT) specimens were desired and from practical standpoint it was not feasible at all. Specimens cost, machine grip, test machine max. pulling capacity and furnace chamber dimensions would not permit this thick specimen to test. Thus, to evaluate the fracture toughness in terms of J_{IC} , 1 inch thick multiple CT specimens were tested using elastic- plastic- fracture- mechanics (EPFM) concept. For high strength superalloys like Alloy 617, two types of testing methods exist, namely single- specimen technique and multiple- specimen technique. Five specimens were needed for multiple specimen technique but only one specimen was required for single specimen technique to determine J_{IC} value in a particular test temperature. All tests were conducted using single specimen technique at temperature ranging from ambient to 500°C. Instron testing machine (max capacity of 100 kN) and J_{IC} fracture toughness software [13] provided by Instron Corporation was used to calculate and validate the fracture toughness value in terms of J_{IC} .

The compact tension specimen was pre-cracked to an approximate of 3 mm at room temperature using a load ratio(R) of 0.1 and frequency of 1 Hz. Maximum load for pre-cracking was maintained at 20 KN and number of cycle for pre-crack ranged from 55000 to 70000. Just after pre-cracking, CT specimens was subjected to 30 loading and unloading cycles to measure load line displacement (LLD) or crack opening displacement (COD). Maximum travel distance of a high temperature knife- edge extensometer was kept ± 2 mm to measure the gap between the pre-cracked specimens. Experimental setup and a standard load versus LLD plot is shown in the Figure 2 and 3 respectively.

The shaded area in Figure 3(b) under the curve represents the energy (J- integral) required to cause each increment of crack length. Fracture toughness value in terms of J- integral for each small area was calculated using the following equations.

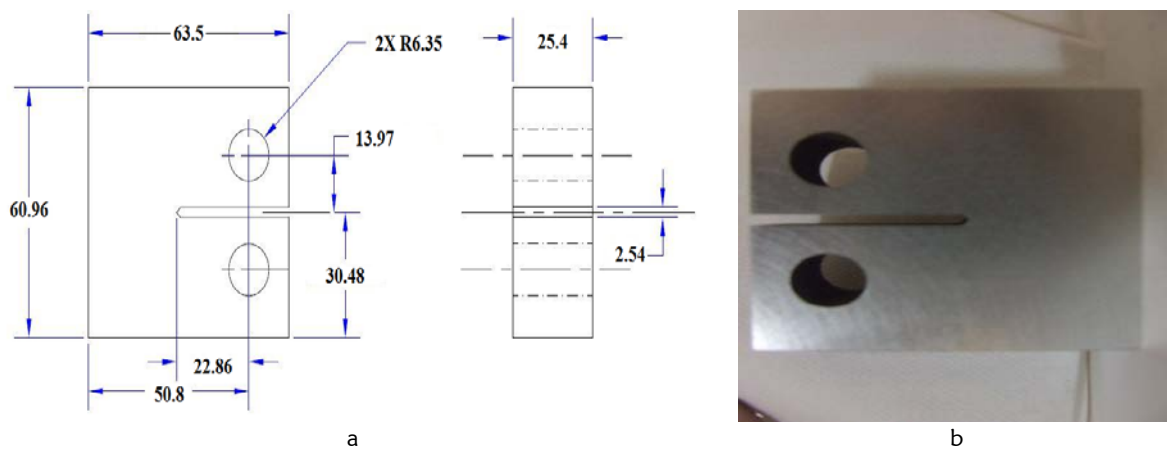


Figure 1: 25.4 mm CT Specimen (a) Specimen Dimensions and (b) Pictorial View

The J-Integral value for each area was calculated using Equations 1-3, given below [12, 14].

$$J = J_{\text{elastic}} + J_{\text{plastic}} \quad [1]$$

$$J_{\text{elastic}} = \frac{K^2}{E} [1 - 2] \quad [2]$$

$$J_{\text{plastic}} = \frac{\eta_{\text{pl}}}{Bb} \int_0^{v_{\text{pl}}} P dv_{\text{pl}} = \frac{\eta_{\text{pl}}}{Bb} \times A_{\text{pl}} \quad [3]$$

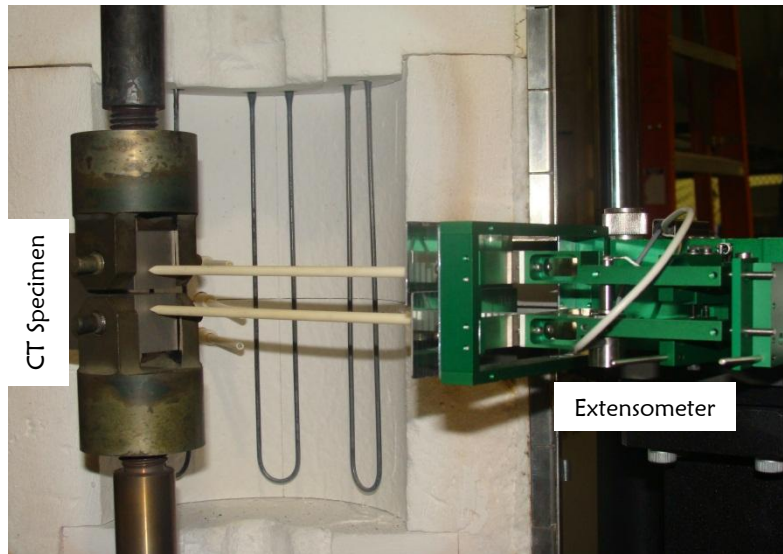


Figure 2: J_{1c} Test Set-up

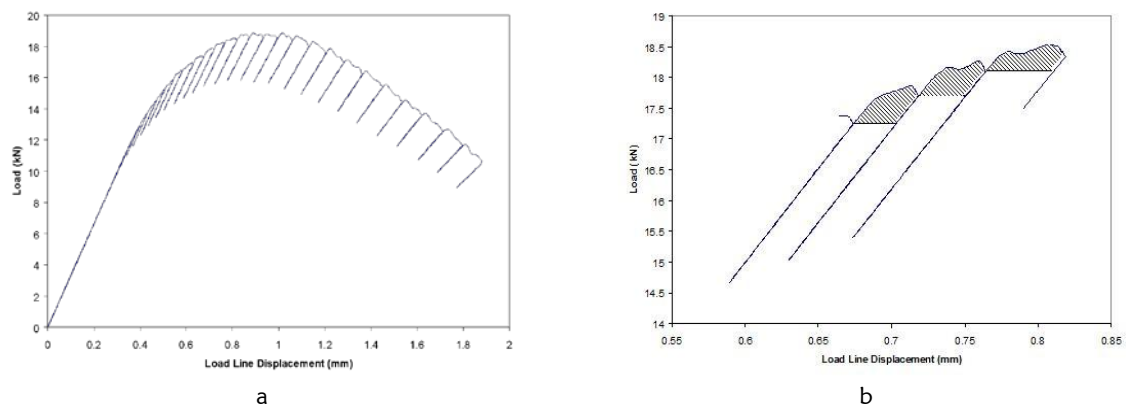


Figure 3: (a) Load versus LLD Plot and (b) Areas Representing J-Integral

where

$$K = \text{Stress intensity factor, MPav/m} = \left[\frac{P}{(BB_N W)^{0.5}} \right] \alpha^x$$

P = Load, N

B = Specimen thickness, mm

B_N = Net specimen thickness, mm = B, in present study

W = Width of the CT specimen, mm

α = Geometric factor of the CT specimen

E = Elastic modulus of the material

ν = Poisson's ratio of the material, 0.3

b = Uncracked ligament, mm

η_{pl} = 2 + 0.522b/W

v_{pl} = LLD / COD, mm

A_{pl} = Area corresponding to each loading / unloading sequence (mm²)

The combined elastic and plastic value of J then plotted against crack extension as shown in Figure 4 Loading compliance principle was used to evaluate each sequence of crack extension (a_i). The following compliance equation 4 was used for a_i calculation [12].

$$a_i/W = 1.000196 - 4.06319u_{LL} + 11.242u_{LL}^2 - 106.043u_{LL}^3 + 464.335u_{LL}^4 - 650.677u_{LL}^5 \tag{4}$$

where

$$u_{LL} = \frac{1}{\left[B_e E C_i \right]^{0.5} + 1}$$

B_e = Effective thickness of the CT specimen, mm = $[B - (B - B_N)^2/B] = B$ (since $B = B_N$), in current study

C_i = Specimen load line elastic compliance on an unloading/reloading sequence ($\Delta v/\Delta P$), mm/N

Δv = Increment in LLD/COD, mm

ΔP = Change in load, N

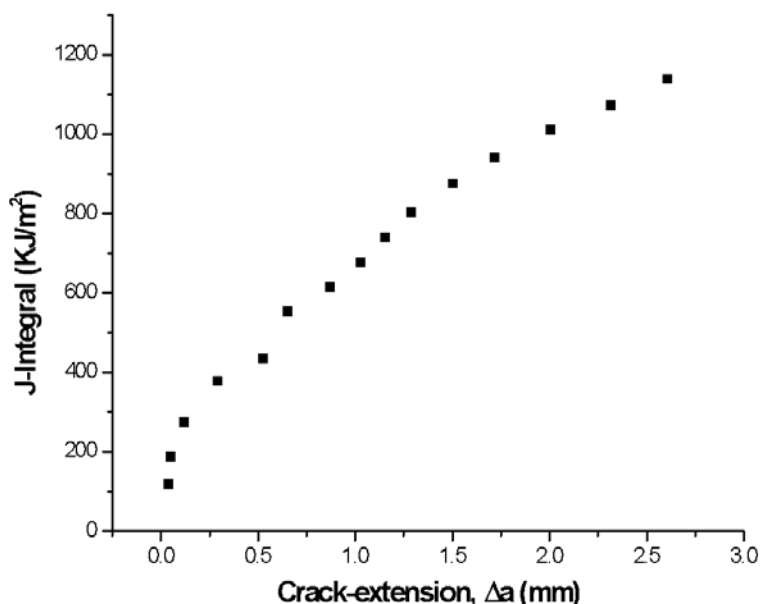


Figure 4: J-Integral vs. Crack-Extension

A power law regeneration curve was plotted in the J-integral versus crack extension (Δa). Four parallel lines including blunting line, 0.15 mm exclusion line, 0.2 mm exclusion line and 1.5 mm exclusion line were superimposed on the plot to find the calculated value of J integral. The plotted value of $J-\Delta a$ can be considered valid if at least one $J-\Delta a$ point lines between 0.15 mm exclusion line and blunting line. The intersection of the 0.2 mm exclusion line and regression curve usually represents the J_Q or conditional J_{IC} value as shown in the Figure 5. Usually J_Q or the conditional J_{IC} value is considered to be the J_{IC} value if the following two criteria are met:

- Thickness (B) of the specimen $> [25 J_Q / \sigma_Y]$, where σ_Y = effective yield strength of the material = average of the yield and ultimate tensile strength (σ_{YS} and σ_{UTS} , respectively) of the material = $[\sigma_{YS} + \sigma_{UTS}] / 2$. Initial uncracked ligament (b_0) $> [25 J_Q / \sigma_Y]$
- Efforts have also been made to correlate J_{IC} to K_{IC} . Literature [15,16] suggests that K_{IC} can be calculated from the J_{IC} value, according to Equation 5, as given below. Fracture toughness can also be measured using the crack-tip-opening-displacement (CTOD) method, which is based on Equation 6, given below [16].

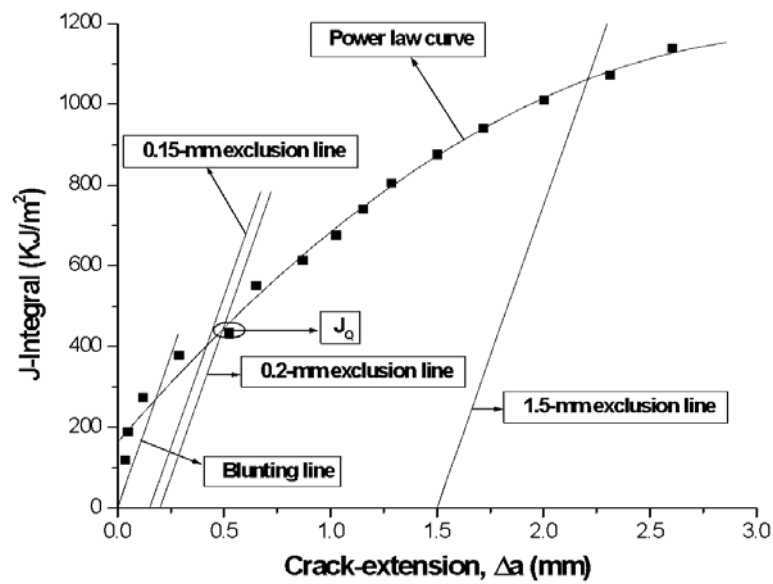


Figure 5: Determination of J_Q Using J-Integral versus Δa Plot

$$K_{IC} = \sqrt{J_{IC} \times E / (1 - \nu^2)} \quad [5]$$

$$\delta = \frac{K_I^2}{m E_{YS}} \quad [6]$$

where

δ = CTOD, mm

K_I = K_{IC} value of the material, MPa \sqrt{m}

m = Constant = 2 for plane-strain condition

Further, tearing modulus has been calculated based on the flow stress and taking into consideration the slopes of the J-integral vs. crack extension curves.

$$\sigma_f = \frac{1}{2} (\sigma_y + \sigma_{UTS}) \quad [7]$$

$$T = \frac{E}{\sigma_f^2} \cdot \frac{dJ}{da} \quad [8]$$

Where,

σ_f = Flow strength

σ_y = Yield strength

σ_{UTS} = Ultimate tensile strength

E = Young's modulus

$\frac{dJ}{da}$ = The slope of the J-integral vs. crack extension curve

3 RESULTS

3.1 J_{IC} values

The validity criteria set by the ASTM Designation E 813-1989 was maintained in the J_{IC} testing procedure. J_Q values were obtained from it. In Figure 6., average J_{IC} values are shown for temperature ranging from 30°C to 300°C. It is observed that J_{IC} values decrease with increasing temperature. The effect is higher for temperature up to 100°C (156 to 103 kJ/m²). However, from 200°C to 300°C, the decrement is insignificant (88 to 86 kJ/m²). Figure 7. displays a load vs. LLD plot and a J-Integral vs. Δa plot is shown in Figure 8.

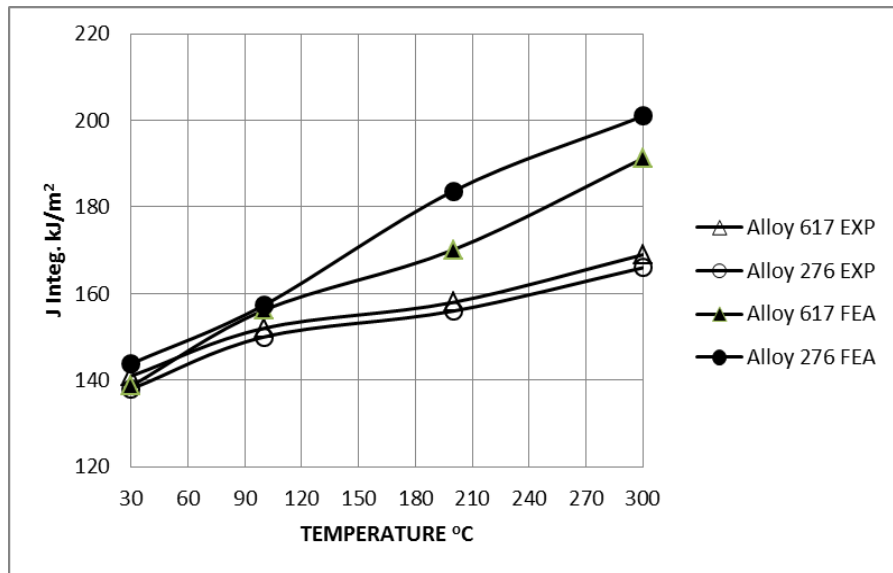


Figure 6: J_{IC} vs. Temperature

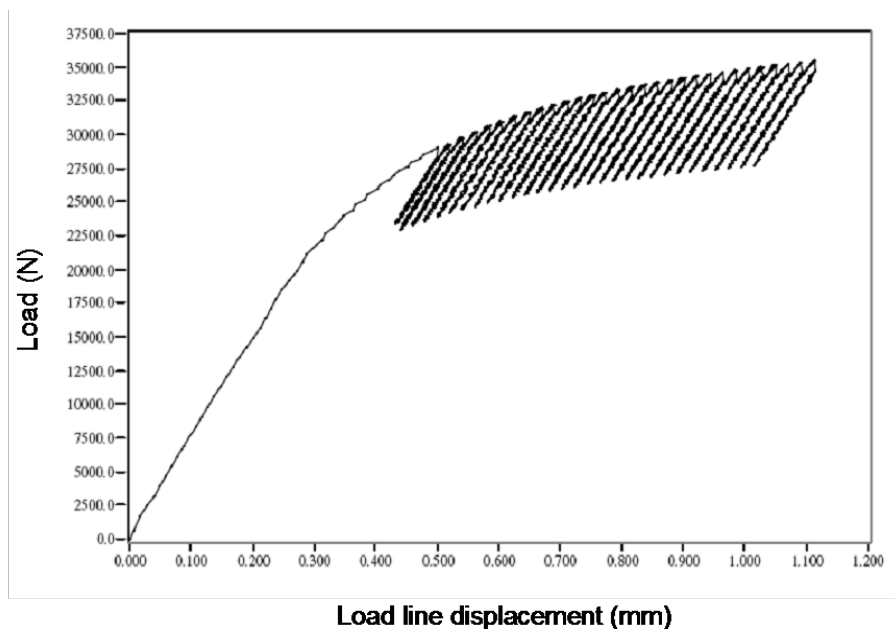
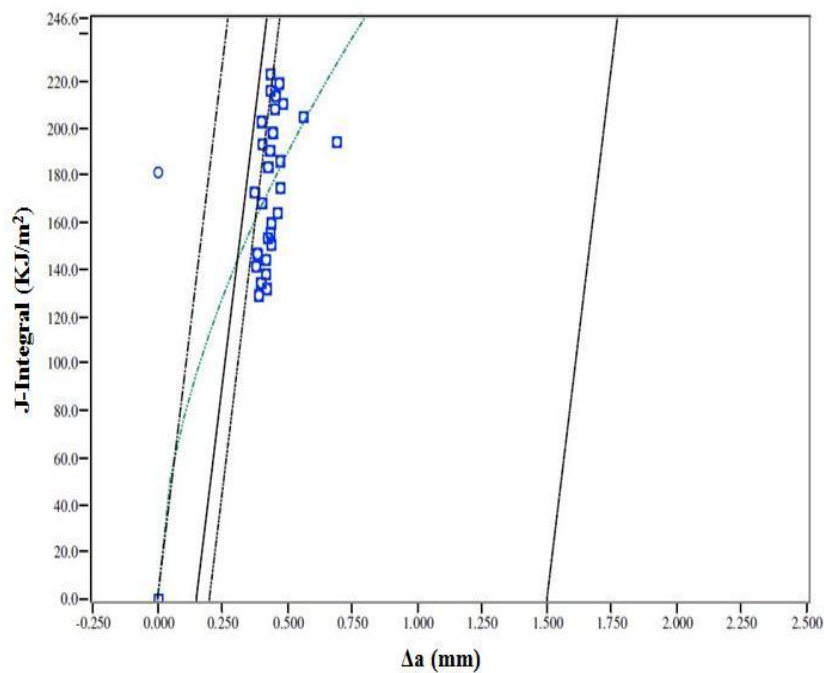


Figure 7: Load vs. LLD at Ambient Temperature



Alloy 617

Figure 8: J-Integral vs. Δa at Ambient Temperature

Table 3: K_{IC} and δ Values vs. Temperature

Temperature (°C)	Alloy 617		Alloy 276	
	K_{IC} (MPa \sqrt{m})	δ (mm)	K_{IC} (MPa \sqrt{m})	δ (mm)
Room Temperature	193.7	0.20	189	0.20
100	208.9	0.22	205.5	0.21
200	216.4	0.23	213.7	0.22
300	231.5	0.24	227.4	0.24

3.2 Equivalent K_{IC} and CTOD values

The fracture toughness values are estimated using the J integral approach. Table 3. shows equivalent K_{IC} and the CTOD values for Alloy 617 and Alloy 276. These values match with open literature. Further, the calculated δ values for alloy 617 were very close to a range in CTOD values (0.1 to 0.2) for an adequately tough material [17].

3.3 Tearing modulus values

The ASTM designation E 8-01 was used to establish the Young’s modulus for Alloy 617. The tearing modulus for this alloy varies with temperature and is represented in a semi-logarithmic scale [18]. By averaging the ultimate tensile strength and yield strength the flow stress is obtained with the highest uncertainty between all conditions. Based on recent research [19] large stretch zone corresponds to large tearing moduli. The furnace setback limited the study to be conducted at a specific temperature range (up to 500°C); however, the tearing modulus maintained to remain close in these temperature constraints resulting, in accurate results corresponding with the study. The values obtained show a high accuracy with the conducted study [19].

3.4 Finite element analysis of experimental work

Half CT specimen shown in Figure.10 has meshed with 1922 quadrilateral 2D solid elements in ANSYS. A load of 30 kN was applied at the inside surface of the specimen hole as shown with arrows. 30 kN load was distributed equally over 15 nodes with each node subjected to 2 kN force. A symmetric boundary condition is shown for the half specimen. Principal stress plots for alloy 276 at room temperature and at 400 °C are shown in Figures 11 and 12 respectively. As expected the plastic zone size at 400 °C is larger compared to the plastic zone size at 30 °C.

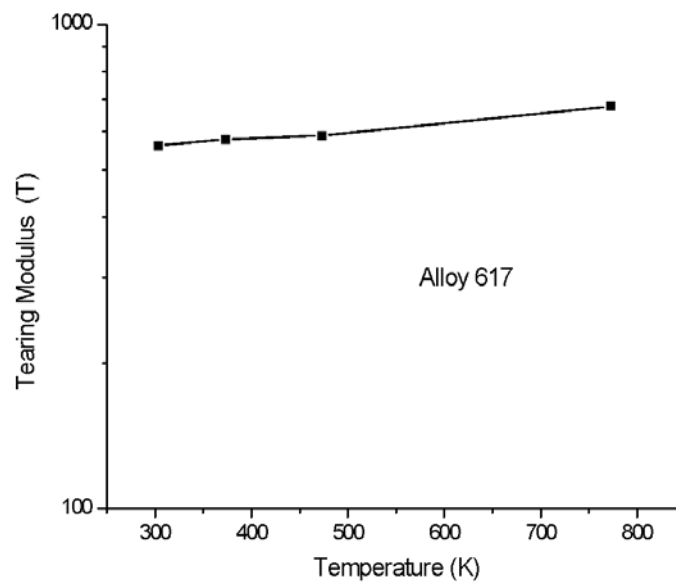


Figure 9: J-Integral vs. Δa at Ambient Temperature

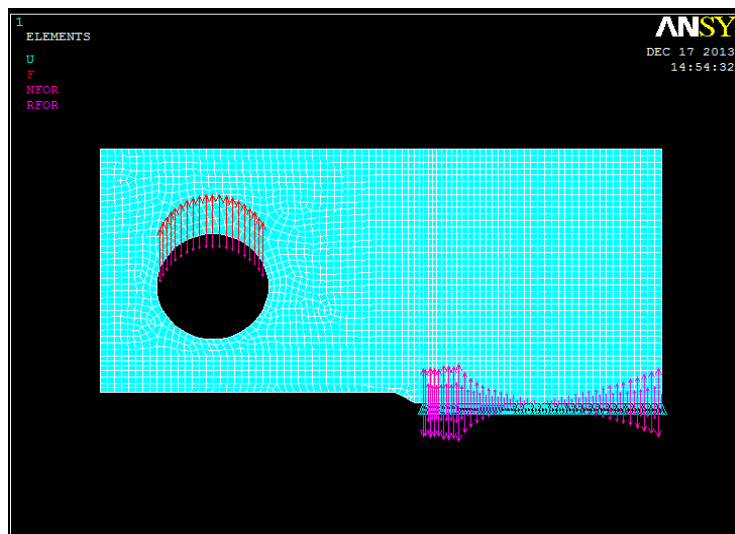


Figure 10: CT specimen mesh showing the loading and the symmetry boundary condition.

A total of 20 paths were defined around the crack tip for J Integral estimation in all simulations. The J Integral values for alloy 617 and alloy 276 at varying temperatures are shown in Fig.13 and Fig.14 respectively. It was observed that as the temperature increases the J values do not converge in the near field paths due to an excessive drop in the yield stress and enhanced plasticity. An increase in J values was recorded for increasing temperatures [20] as shown in Fig.14. That also points out to the fact that the path independency of the J integral could not be maintained at higher plasticity [21]. This is shown in Fig.14 where the J values do not converge easily to a single value but show a path dependency at 400 °C. Path independency for J integral was observed even until 500 °C for the alloy 617 but as the temperature reaches 400 °C for alloy 276 the J values show path dependence. Cracking deformation behaviour in nickel-based superalloys with stress and strain characteristics are correlated by finite element analysis of microscopic and macroscopic structures [10].

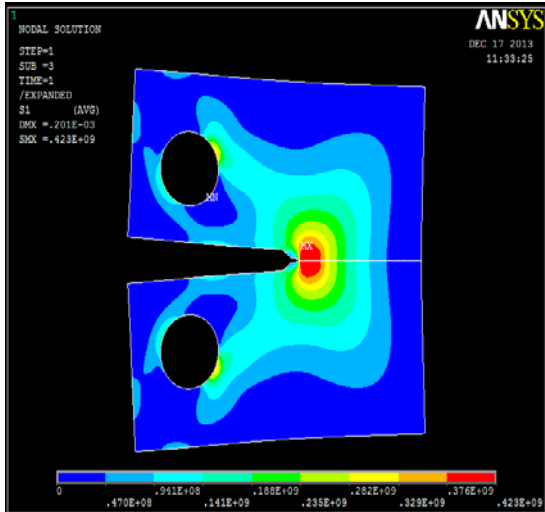


Figure 11: Principal stress distribution in CT specimen for Alloy 276 at 30 °C

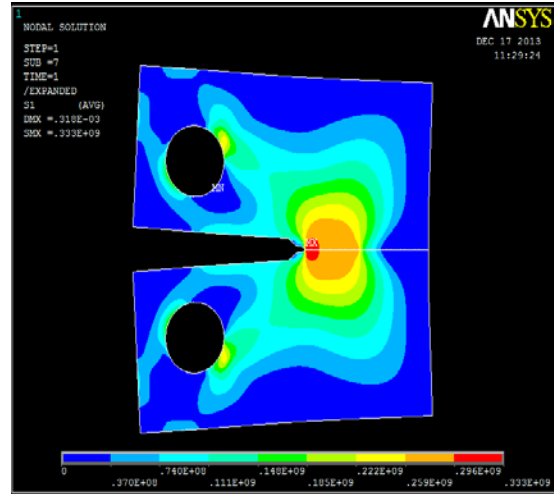


Figure 12: Principal stress distribution in CT specimen for Alloy 276 at 400 °C

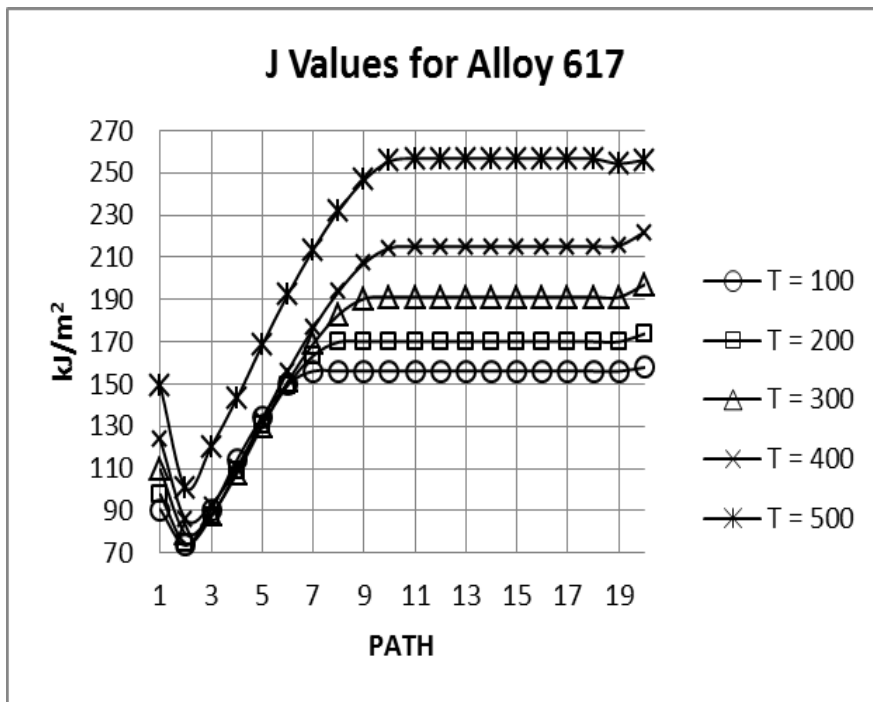


Figure 13: J Integral variation with increasing temperature for alloy 617.

3.5 Fractographic Evaluations

Figure 15 indicates the SEM micrographs of alloy 617 that were sampled and experimented at room temperature. Three different sections are illustrated by the micrographs each causing a change in morphology. Fatigue precracking results in mild striations in one region; however, the vivid striations are caused by loading and unloading sequences and the last region shows dimples on the surface which result from fast rupture. Changes in microstructure, as well as applied strain range due to high temperatures, causes a decline in fatigue life in Alloy 617 [22].

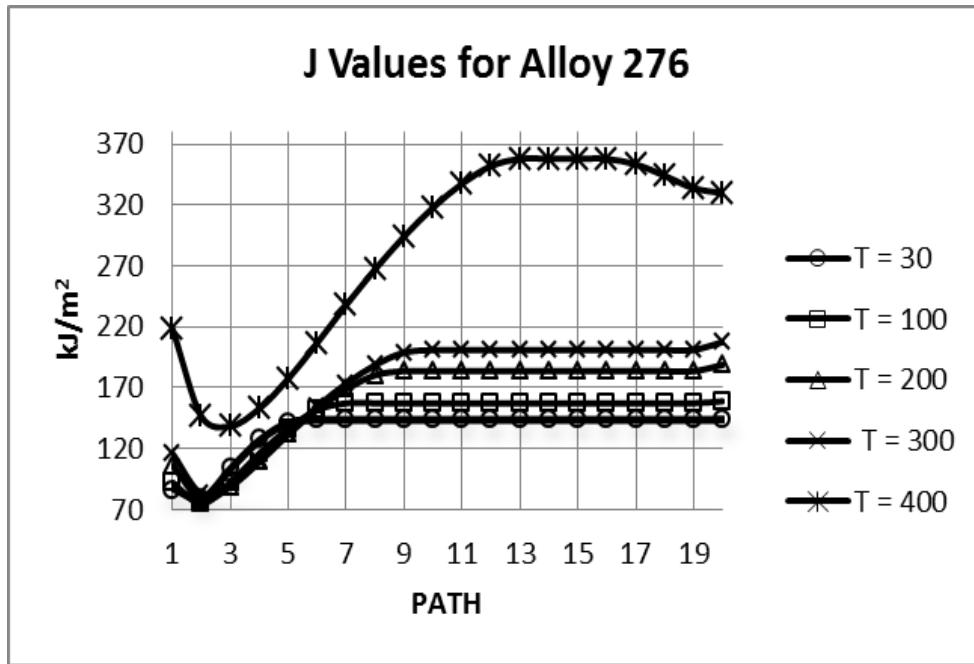


Figure14: J Integral variation with increasing temperature for alloy 276

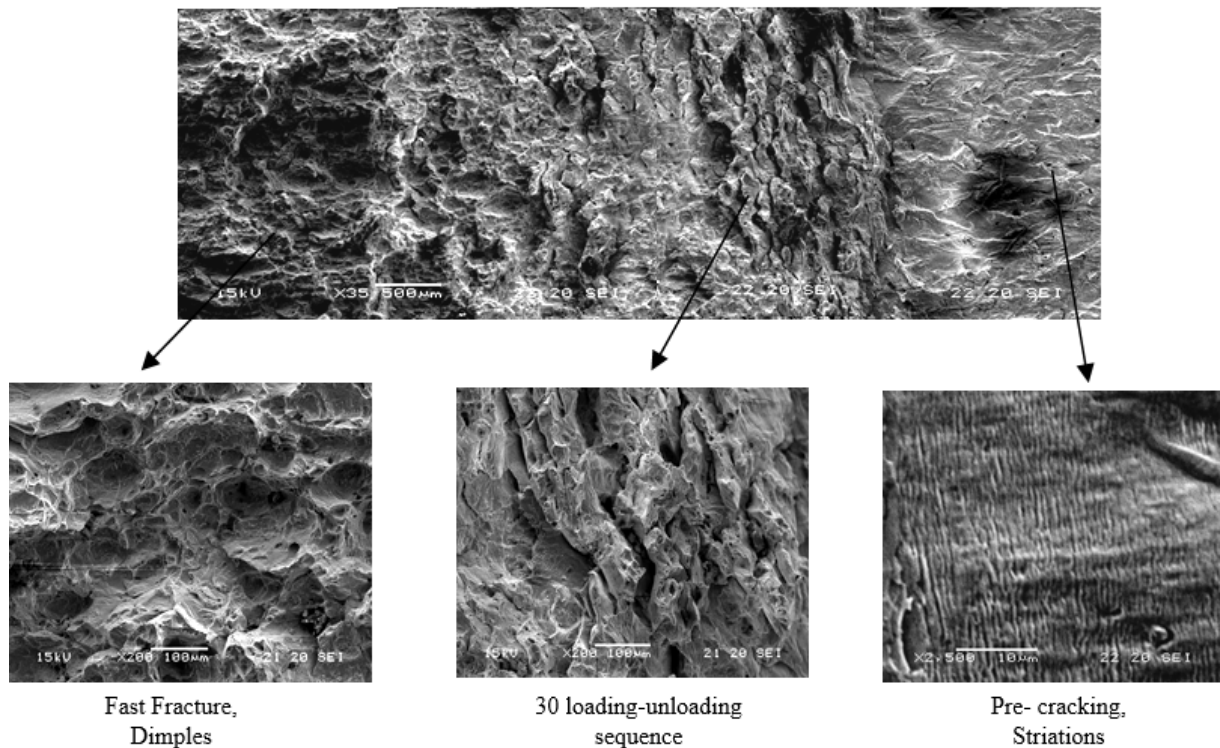


Figure 15: SEM micrographs of sampled specimens

4 CONCLUSIONS

The focus of this study was on the evaluation of fracture toughness behaviour of Alloys 617 and 276. The key results obtained from the investigation are summarized below.

1. The J_{IC} values fulfilled the legitimacy requirements dictated by the ASTM Designation E 813-1989.
2. The effect of temperature on J_{IC} value for Alloy 617 is not that much significant up to 500°C. The reduction in the J_{IC} value from 200 to 500°C was minimal. Further, the tearing modulus was changed insignificantly along with the temperature as expected.
3. An abrupt increase is observed in the value of J_{IC} for Alloy 276 from 400°C temperature to 500°C, due to enhanced plasticity and path dependency.
4. J values for both the alloys show path independency up to 300° C for an insignificant amount of plastic zone at the crack tip.
5. Experimental results of J values and path independency were validated by the finite element analysis in ANSYS.
6. Dimpled microstructures and striations are revealed from the fractographic evaluations of both broken CT specimens.

ACKNOWLEDGEMENT

The authors would like to appreciate very much the experimental and analytical support from Department of Mechanical and Industrial Engineering at Ryerson University in doing this research.

REFERENCES

1. N. Dalili, A. Edrisy and R. Carriveau "A review of surface engineering issues critical to wind turbine performance" *Renewable and Sustainable energy reviews*, 13 (2009) 428-438.
2. Paul M. Mathias and Lloyd C. Brown "Thermodynamics of the Sulfur-Iodine Cycle for Thermochemical Hydrogen Production" Japan March 2003, 68th Annual Meeting of the Society of Chemical Engineers, Japan The University of Tokyo
3. Akbari-Garakani, M., & Mehdizadeh, M. (2011). Effect of long-term service exposure on microstructure and mechanical properties of alloy 617. *Materials and Design*, 32(5), 2695-2700. doi:10.1016/j.matdes.2011.01.017
4. Y. Sakai, T. Tanabe, T. Suzuki, H. Yoshida, "Corrosion Behavior of Inconel 617 in a Simulated HTGR Helium", *Transactions of National Research Institute for Metals*, vol. 27, 1985, pp. 20-27
5. U. Bruch, D. Schumacher, P. Ennis, E. Heesen, "Tensile and Impact Properties of Candidate Alloys for High-Temperature Gas-Cooled Reactor Applications", *Nuclear Technology*, vol. 66, 1984, pp. 357-362
6. Ajit Roy, Muhammad H. Hasan, Joydeep Pal "Creep deformation of Nickel-base superalloys at different temperatures", *Materials science and Engineering: A* 520 (2009) 184-188.
7. Yu, Q. M., Hou, N. X., & Yue, Z. F. (2010). Finite element analysis of void growth behavior in nickel-based single crystal superalloys. *Computational Materials Science*, 48(3), 597-608. doi:10.1016/j.commatsci.2010.02.028
8. Vikram Marthandam, "Tensile Deformation, Toughness and Crack Propagation Studies of Alloy 617", Ph.D. Dissertation, Mechanical Engineering, April 10, 2008
9. "Wan, V. V. C., Jiang, J., MacLachlan, D. W., & Dunne, F. P. E. (2016). Microstructure-sensitive fatigue crack nucleation in a polycrystalline ni superalloy. *International Journal of Fatigue*, 90, 181-190. doi:10.1016/j.ijfatigue.2016.04.013"
10. Mukai, Y., Kagawa, H., & Okazaki, M. (2015). Finite element analysis on crack tip deformation behavior under mode-II loading in single crystal superalloy. *Key Engineering Materials*, 665, 281-284.
11. Xiao Guang, Zu Han Lai, "Realization of single specimen analytical method of J_{IC} determination by using compact tension loading". *Engineering Fracture Mechanics*, Vol 34 No.5/6, pp 1013-1021, 1989
12. ASTM Designation E 399-1999. "Standard Test Method for Linear-Elastic Plane-Strain Fracture Toughness K_{IC} of Metallic Materials." American Society for Testing and Materials (ASTM) International
13. ASTM Designation E 813-1989. "Standard Test Method for J_{IC} , A Measure of Fracture Toughness." American Society for Testing and Materials (ASTM) International.
14. Instron Corp. Fast Track 2 - J_{IC} Unloading Compliance Software.
15. Structural Integrity Associates Inc. "Nonlinear Fracture Toughness Testing." Technical Paper.
16. Perez, J.E., Ipiñaa, Yawnyb, A.A., Stukeb, R. & Oliverb, C. Gonzalez. "Fracture Toughness in Metal Matrix Composites." *Materials Research* 3 (2000): 74-78.
17. Hertzberg, Richard W. *Deformation and Fracture Mechanics of Engineering Materials*. NY: John Wiley & Sons, 1996.
18. ASTM Designation E 8-2001. "Standard Test Method for Tension Testing of Metallic Materials"
19. K. Krompholz, E.D. Grosser & K.Ewert. "Determination of J-integral R-curve for Hastelloy X and Inconel 617 up to 1223 K using Potential Drop Technique" *Materials Science and Engineering Technology*, Volume 13, Issue 7, Page 236-244, July 1982.

20. Hsiao-Hung Hsu, Yen-Chie Wu, Leu-Wen Tsay, Notch brittleness of Ti-15V-3Cr-3Al alloys, *Materials Science and engineering A*, 545 (2012) 20-25.
21. W. Brocks and I. Scheider, Numerical Aspects of the Path-Dependence of the J-Integral in Incremental Plasticity: How to calculate reliable J-values in FE analyses, Technical Note GKSS/WMS/01/08, internal report, Institut für Werkstofforschung. (2001)
22. Dewa, R. T., Kim, S. J., Kim, W. G., & Kim, E. S. (2017). Effect of strain range on the low cycle fatigue in alloy 617 at high temperature. *Metals*, 7(2), 54. doi:<http://dx.doi.org.ezproxy.lib.ryerson.ca/10.3390/met7020054>
23. Riveros, G. A. , Numerical evaluation of stress intensity factors (KI) J-integral approach. Coastal and Hydraulics Engineering Technical Note, ERDC/CHL CHETN-IX-16. (2006) Vicksburg, MS: U.S. Army Engineer Research and Development Center.
24. H Ching, C Liu, S Yen, FE calculations of J-Integrals in a constrained elastomeric disk with crack surface pressure and isothermal load, Air Force Research Laboratory (AFMC),AFRL/PRSM,10 E. Saturn Blvd.,Edwards (2004) AFB,CA,93524-7680
25. "CTOD Testing." May 25, 2009. <<http://www.twi.co.uk/content/jk76.html>>.